Particle number conserving BCS approach in the relativistic mean field model and its application to $^{32-74}$Ca*

Rong An(安荣)[1] Lisheng Geng(耿立升)[2;1)] Shisheng Zhang(张时声)[1;2)] Lang Liu(刘朗)[3;3)]

[1] School of Physics and Nuclear Energy Engineering, Beihang University, Beijing 100191, China
[2] School of Physics and Nuclear Energy Engineering & Beijing Key Laboratory of Advanced Nuclear Materials and Physics, Beihang University, Beijing 100191, China
Beijing Advanced Innovation Center for Big Data-based Precision Medicine, Beihang University, Beijing 100191, China
[3] School of Science, Jiangnan University, Wuxi 214122, China

Abstract: A fixed particle number BCS (FBCS) approach is formulated in the relativistic mean field (RMF) model. It is shown that the RMF+FBCS model obtained can describe the weak pairing limit. We calculate the ground-state properties of the calcium isotopes $^{32-74}$Ca and compare the results with those obtained from the usual RMF+BCS model. Although the results are quite similar to each other, we observe the interesting phenomenon that for ^{54}Ca, the FBCS approach can enhance the occupation probability of the $2p_{1/2}$ single particle level and slightly increases its radius, compared with the RMF+BCS model. This leads to the unusual scenario that although ^{54}Ca is more bound with a spherical configuration, the corresponding size is not the most compact. We anticipate that such a phenomenon might happen for other neutron-rich nuclei and should be checked by further more systematic studies.

Keywords: relativistic mean field model, pairing correlation, BCS approach, particle number projection

PACS: 21.10.-k, 21.60.Jz **DOI:** 10.1088/1674-1137/42/11/114101

1 Introduction

In recent years, studies of exotic nuclei with large isospin ratios have been at the forefront of nuclear physics both theoretically and experimentally (see, e.g., Refs. [1, 2] and references therein). This brings great challenges to existing nuclear structure models for the reliable understanding, interpretation and prediction of new experimental phenomena. Two of the crucial theoretical issues (at least in mean-field models) are: (i) a proper description of the continuum; and (ii) a reliable treatment of the residual pairing correlation. Both subjects have been extensively studied [3–14]. The pairing correlation has long been known to be essential to describe many experimental observables, such as moments of inertia, level densities, and energies of the lowest-lying excited states [15, 16]. It plays an more important role for some weakly bound nuclei, where it is essential for their existence in mean-field models.

Conventionally, the pairing correlation can be treated either by the Bardeen-Cooper-Schrieffer (BCS) [17–19] method or by the Bogoliubov transformation [20]. In earlier days, it was realized that these methods, originally developed for macroscopic systems, result in spurious sharp phase transitions from normal states to superfluid states [19], which have never been observed in experiments. The sharp phase transitions are due to the breaking of particle number conservation in finite nuclei and the fact that only the expectation value of the particle number operator is fixed. In a macroscopic system, this can be safely ignored since the particle number is large enough. However, in a microscopic system, such as an atomic nucleus, it can lead to spurious effects which should be carefully studied. These early findings have led to a lot of efforts in developing alternative approaches which improve the treatment of the pairing correlation. The generally accepted approach to restore the broken gauge symmetry of particle number is the projection technique, see e.g., Refs. [21–26]. The differences among the various treatments have been studied in much detail. It is found that most treatments are quite similar to each other in the strong pairing limit, while only the variation after projection methods can properly describe the weak pairing limit.

Received 6 May 2018, Published online 25 September 2018
∗ Supported by the National Natural Science Foundation of China (11522539, 11735003, 11775014, 11375022)
1) E-mail: lisheng.geng@buaa.edu.cn
2) E-mail: zss76@buaa.edu.cn
3) E-mail: liulang@jiangnan.edu.cn

A pairing method which conserves the gauge symmetry of particle number is particularly desirable for weakly bound nuclei because (i) the pairing correlation plays an important role in binding the whole nucleus and (ii) only a few single particle levels around the Fermi surface are important for the pairing correlation [10][1)]. Therefore, it will be very interesting to formulate such a method within a reliable mean-field model and study its impact on relevant physical quantities. In the present work, we formulate the fixed particle number BCS (FBCS) method [21] in the relativistic mean field model, one of the two most successful mean field models [27]. To our knowledge, so far, only the Lipkin-Nogami BCS method [28, 29], the exact approach [30], and the shell-model-like approach (SLAP) [31–33] have been explored in the relativistic mean field model.

This paper is organized as follows. In Section 2, we briefly review the relativistic mean field (RMF) model. In Section 3, we introduce the FBCS method and its implementation in the relativistic mean field model. In Section 4, we explain how the residuum integrals are solved numerically. In Section 5, we study the general features of the RMF+FBCS model by comparing its results with those of the RMF+BCS model. In Section 6, we check how well the ground-state properties of the calcium isotopes can be described by these two different approaches. Finally, we summarize and point out possible future extensions in Section 7.

2 The relativistic mean field model

The basic assumptions made in the relativistic mean field model are that the nucleons are point-like Dirac fermions and their interactions are mediated via meson exchanges. One can then write down the relativistic Lagrangian densities for both nucleons and mesons as well as photons. Adopting the so-called mean-field and no-sea approximations, one then solves the coupled equations self-consistently. For a more detailed explanation of the RMF model and the recent developments, see, e.g., Refs. [34–40].

The Lagrangian density used in this study has the following form:

$$\begin{aligned}\mathcal{L} = \bar{\psi}[&i\gamma^\mu\partial_\mu - M - g_\sigma\sigma - \gamma^\mu(g_\omega\omega_\mu + g_\rho\vec{\tau}\cdot\vec{\rho}_\mu \\ &+ e\frac{1-\tau_3}{2}A_\mu) - \frac{f_\pi}{m_\pi}\gamma_5\gamma^\mu\partial_\mu\vec{\pi}\cdot\vec{\tau}]\psi \\ &+ \frac{1}{2}\partial^\mu\sigma\partial_\mu\sigma - \frac{1}{2}m_\sigma^2\sigma^2 - \frac{1}{3}g_2\sigma^3 - \frac{1}{4}g_3\sigma^4 \\ &- \frac{1}{4}\Omega^{\mu\nu}\Omega_{\mu\nu} + \frac{1}{2}m_\omega^2\omega_\mu\omega^\mu + \frac{1}{4}c_3(\omega^\mu\omega_\mu)^2 \\ &- \frac{1}{4}\vec{R}_{\mu\nu}\cdot\vec{R}^{\mu\nu} + \frac{1}{2}m_\rho^2\vec{\rho}^\mu\cdot\vec{\rho}_\mu + \frac{1}{4}d_3(\vec{\rho}^\mu\vec{\rho}_\mu)^2 \end{aligned} \quad (1)$$

where all symbols have their usual meanings. The corresponding Dirac equation for the nucleons and the Klein-Gordon equations for the mesons and photon, obtained with the mean-field and the no-sea approximation, are solved by the expansion method with the harmonic oscillator basis [11, 41, 42]. In the present work, 12 shells are used to expand the Fermi fields and 20 shells for the meson fields. The mean-field effective force used is NL3 [43], and we found that using other effective forces such as TM1 [44] and PK1 [45] do not essentially change any of our conclusions.

3 The FBCS method

The FBCS method has been known for a long time [21], but to our knowledge, it has not been applied in the relativistic mean field model in a self-consistent manner. Here we briefly describe some essential ingredients of this approach. A detailed derivation can be found in Ref. [21]. In order to simplify the final FBCS equations and also to simplify the derivation, we adopt the notion of the "residuum integrals" introduced by Dietrich, Mang and Pradal [21]. Introducing a complex variable $z=\mathrm{e}^{\mathrm{i}\psi}$, the number projection operator can be written as an integral in the complex plane:

$$\hat{P}^N = \frac{1}{2\pi i}\oint \frac{z^{\hat{N}}}{z^{N+1}}\mathrm{d}z. \quad (2)$$

Here we note the property $\oint \frac{\mathrm{d}z}{z^n} = 2\pi i\delta_{n1}$ with the contour being taken around the origin. When applied to the BCS wave function of the following form

$$|\Psi\rangle = |BCS\rangle = \prod_{k>0}(u_k + v_k\hat{c}_k^\dagger\hat{c}_{\bar{k}}^\dagger)|0\rangle, \quad (3)$$

one obtains the projected wave function

$$|\Psi_N\rangle = \frac{1}{2\pi i}\oint \frac{\mathrm{d}\xi}{\xi^{p+1}}\prod_{k>0}(u_k + v_k\xi\hat{c}_k^\dagger\hat{c}_{\bar{k}}^\dagger)|0\rangle, \quad (4)$$

where we have introduced $\xi = z^2$ and used the fact that the pair operator $\hat{c}_k^\dagger\hat{c}_{\bar{k}}^\dagger$ raises the particle number by 2, and $p = N/2$ is the number of nucleon pairs. Also, we have used the property $\oint \frac{\mathrm{d}\xi}{\xi} = 2\pi i$. The integrand in the above equation is a Laurent series in ξ. The integration just picks the terms with ξ^{-1}, which is the component with p pairs. Using the fermion anti-commutation relations for the operators $\hat{c}_k$ and $\hat{c}_k^\dagger$, arbitrary matrix elements can be expressed by the residuals:

$$R_\nu^m(k_1,\cdots,k_m) = \frac{1}{2\pi i}\oint \frac{\mathrm{d}z}{z^{(p-\nu)+1}}\prod_{k\neq k_1,\cdots,k_m>0}(u_k^2 + zv_k^2), \quad (5)$$

1) For a relevant discussion on the difference between the BCS and Bogoliubov approaches in the non-relativistic framework, see, e.g., Ref. [3].

where the product under the integral is over the whole pairing space, the m states listed in the argument of $R(\cdots)$ are to be excluded from the product, and $p-\nu$ is the effective number of nucleon pairs, with ν an integer. Suppose that the Hamiltonian of the system has the following form [15, 16] (a single particle part plus a pure pairing part):

$$\begin{aligned}\hat{H} &= \sum_{j>0}\varepsilon_j(\hat{c}_j^\dagger\hat{c}_j+\hat{c}_{\bar{j}}^\dagger\hat{c}_{\bar{j}}) \\ &\quad+\sum_{j_1,j_2>0}\bar{V}_{j_1,\bar{j_1},j_2,\bar{j_2}}\hat{c}_{j_1}^\dagger\hat{c}_{\bar{j_1}}^\dagger\hat{c}_{\bar{j_2}}\hat{c}_{j_2}. \end{aligned} \tag{6}$$

The total energy of the system, which is the expectation value of the Hamiltonian, can be expressed as

$$\begin{aligned}E_{\rm proj}^N &= \frac{\langle\Psi_N|\hat{H}|\Psi_N\rangle}{\langle\Psi_N|\Psi_N\rangle} \\ &= 2\sum_{j>0}\varepsilon_j v_j^2\frac{R_1^1(j)}{R_0^0}+\sum_{j>0}\bar{V}_{j,\bar{j},j,\bar{j}}v_j^4\frac{R_1^1(j)}{R_0^0} \\ &\quad+\sum_{j_1,j_2>0}\bar{V}_{j_1,\bar{j_1},j_2,\bar{j_2}}u_{j_1}v_{j_1}u_{j_2}v_{j_2}\frac{R_1^2(j_1,j_2)}{R_0^0}. \end{aligned} \tag{7}$$

In the second step, we have used the relation $R_\nu^2(k,k)=R_1^1(k)$ [15]. From now on, we adopt a different notation for the pairing matrix element, $G_{j_1j_2}=-\bar{v}_{j_1,\bar{j_1},j_2,\bar{j_2}}$. Then the energy of the system can be expressed as

$$\begin{aligned}E_{\rm proj}^N &= \sum_{j\neq k>0}2\left[\left(\varepsilon_j-\frac{1}{2}G_{jj}v_j^2\right)v_j^2\right]\frac{R_1^2(j,k)}{R_0^0} \\ &\quad-\sum_{j_1>0}\sum_{j_2>0}G_{j_1j_2}u_{j_1}v_{j_1}u_{j_2}v_{j_2}\frac{R_1^2(j_1.j_2)}{R_0^0} \\ &= \sum_{j>0}2E_jv_j^2\frac{R_1^1(j)}{R_0^0}-\sum_{j>0}\Delta_ju_jv_j, \end{aligned} \tag{8}$$

where Δ_j is defined below and we have introduced a new quantity $E_j=\varepsilon_j-\frac{1}{2}G_{ij}v_j^2$. In the BCS treatment, the second term $-\frac{1}{2}G_{ij}v_j^2$ is usually neglected with the argument that it corresponds only to a renormalization of the single particle energies. In that case E_j is simply ε_j. This approximation is also adopted in our present work. A variation of the projected energy with respect to u_j and v_j,

$$\left(\frac{\partial}{\partial v_j}-\frac{v_j}{u_j}\frac{\partial}{\partial u_j}\right)E_{\rm proj}^N=0, \tag{9}$$

leads to the FBCS equation

$$2(\widetilde{\varepsilon_j}+\Lambda_j)u_jv_j+\Delta_j(v_j^2-u_j^2)=0. \tag{10}$$

The quantities $\tilde{\varepsilon}_j$, Λ_j and Δ_j are defined as follows:

$$\begin{aligned}\widetilde{\varepsilon_j} &= (\varepsilon_j-G_{jj}v_j^2)\frac{R_1^1}{R_0^0}, \\ \Delta_j &= \sum_{k>0}G_{jk}u_kv_k\frac{R_1^2(j,k)}{R_0^0}(v_j^2-u_j^2), \\ \Lambda_j &= \sum_{k>0}\left(\varepsilon_j-\frac{1}{2}G_{kk}v_k^2\right)v_k^2\frac{R_0^0(R_2^2-R_1^2)-R_1^1(R_1^1-R_0^1)}{(R_0^0)^2} \\ &\quad-\frac{1}{2}\sum_{k_1,k_2>0}G_{k_1k_2}u_{k_1}v_{k_1}u_{k_2}v_{k_2}\frac{R_0^0(R_2^3-R_1^3)}{(R_0^0)^2} \\ &\quad+\frac{1}{2}\sum_{k_1,k_2>0}G_{k_1k_2}u_{k_1}v_{k_1}u_{k_2}v_{k_2}\frac{R_1^2(R_1^1-R_0^1)}{(R_0^0)^2}. \end{aligned} \tag{11}$$

The quantity Λ_j has no counterpart in the conventional BCS equation, where a constant chemical potential is chosen to make the expectation value of the number operator equal to the required particle number. In the derivation of the above equation, the quantity Λ_j arises from the differentiation of the residuum integrals with respect to v_j and u_j. In the usual BCS theory, v_j^2 is the probability of the pair of states $(j,\bar{j})$ being occupied, and u_j^2 is the probability of this pair of states being unoccupied. In the FBCS theory, the corresponding quantities ϵ_j^2 and f_j^2 are:

$$\epsilon_j^2=\langle\Psi_N|(\hat{c}_j\hat{c}_{\bar{j}})^\dagger(\hat{c}_j\hat{c}_{\bar{j}})|\Psi_N\rangle=v_j^2R_1^1(j)/R_0^0, \tag{12}$$

$$f_j^2=1-\epsilon_j^2=u_j^2R_0^1(j)/R_0^0. \tag{13}$$

To derive the above relations, we have used the recursion relations and derivatives of the "residuum integrals" [21]. Of course, the sum of the occupation probabilities is equal to $N/2$, i.e., the number of pairs of particles:

$$\sum_{j>0}\epsilon_j^2=N/2=p. \tag{14}$$

The solutions of the FBCS equation can be formally expressed as:

$$\begin{aligned}u_j^2 &= \frac{1}{2}\left(1-\frac{\widetilde{\varepsilon_j}+\Lambda_j}{\sqrt{(\widetilde{\varepsilon_j}+\Lambda_j)^2+\Delta_j^2}}\right), \\ v_j^2 &= \frac{1}{2}\left(1+\frac{\widetilde{\varepsilon_j}+\Lambda_j}{\sqrt{(\widetilde{\varepsilon_j}+\Lambda_j)^2+\Delta_j^2}}\right), \end{aligned} \tag{15}$$

which have the same form as the solutions of the conventional BCS equation, but with $\widetilde{\varepsilon_j}$ instead of ε_j.

The total energy in the RMF+BCS model can be expressed simply as

$$E=E_{\rm RMF}+E_{\rm pair}^p+E_{\rm pair}^n, \tag{16}$$

with the pairing energy

$$E_{\rm pair}=-\sum_{k>0}\Delta_ku_kv_k. \tag{17}$$

In the usual RMF+BCS model, the densities are determined by the occupation probabilities v_i^2 multiplied by

$|\psi_j|^2$, the modulus of the occupied single particle wave functions. In the RMF+FBCS model, we merely replace the occupation probabilities v_i^2 by $f_i^2 = v_i^2 R_1^1/R_0^0$, i.e.

$$\sum_i v_i^2 \cdots \Rightarrow \sum_i f_i^2 \cdots . \tag{18}$$

4 Evaluation of the residuum integrals

To solve the FBCS equation, one needs to calculate the residuum integrals, i.e. R_0^0, R_0^1, R_1^1, R_1^2, R_2^2, R_1^3 and R_2^3. One can simplify the calculations by reducing the number of residuum integrals with several recursion relations. The first one is given by Dietrich et al. [21], i.e.,

$$\begin{aligned} R_\nu^m(k_1,\cdots,k_m) = {} & R_{\nu+1}^{m+1}(k_1,\cdots,k_m,k)v_k^2 \\ & + R_\nu^{m+1}(k_1,\cdots,k_m,k)u_k^2. \end{aligned} \tag{19}$$

With this relation, one third of the total number of independent residuum integrals can be reduced. Another more powerful relation, first deduced by Ma et al. [46], is

$$\begin{aligned} R_\nu^m(k_1,\cdots,k_m) = {} & \delta_{m\nu} R_0^0 \prod_{i=k_1,\cdots,k_m} \frac{1}{v_i^2} \\ & + (-1)^\nu \sum_{i=k_1,\cdots,k_m} v_i^{2(m-\nu-1)} u_i^{2\nu} \\ & \times \left(\prod_{j=k_1,\cdots,k_m \neq i} \frac{1}{v_i^2 - v_j^2} \right) R_0^1(i). \end{aligned} \tag{20}$$

The remaining residuum integrals,

$$R_\nu^m(k_1,\cdots,k_m) = \frac{1}{2\pi i} \oint \frac{\mathrm{d}z}{z^{(p-\nu)+1}} \prod_{k\neq k_1,\cdots,k_m>0} (u_k^2 + z v_k^2), \tag{21}$$

can be calculated straightforwardly by replacing z with $r(\cos\theta + i\sin\theta)$, namely,

$$\begin{aligned} R_\nu^m(k_1,\cdots,k_m) = {} & \frac{1}{2\pi i} \oint \frac{r(-\sin\theta + i\cos\theta)\mathrm{d}\theta}{[r(\cos\theta + i\sin\theta)]^{(p-\nu)+1}} \\ & \times \prod_{k\neq k_1,\cdots,k_m>0} [u_k^2 + r(\cos\theta + i\sin\theta) v_k^2]. \end{aligned} \tag{22}$$

5 General features of the RMF+FBCS model

In this section, we study the general features of the RMF+FBCS model and compare them with those of the conventional RMF+BCS model. For such a purpose, we take the calcium isotopes $^{32-74}$Ca as examples. We adopt the commonly used density-independent contact delta interaction $V = -V_0\delta(\vec{r}_1 - \vec{r}_2)$ for the particle-particle channel in both methods. The only free parameter in the pairing channel is the pairing strength V_0, which can be fixed by fitting the pairing gap (Δ) to the experimental odd-even mass difference. The single particle levels active for the pairing correlation are confined to those within a 10 MeV window around the Fermi surface.

The FBCS method is expected to be able to provide a smooth phase transition from normal states to superfluid states as a function of the pairing strength. This is very important because it can show whether the FBCS method can properly describe the weak pairing limit. In Fig. 1, the neutron pairing energy of ^{36}Ca is plotted as a function of the pairing strength V_0. Clearly, the FBCS method does lead to non-trivial solutions no matter how weak the pairing strength, while an abrupt transition between superfluid and normal states arises in the BCS method. The BCS equation completely fails to give a non-trivial solution below the critical pairing strength of about 250 MeV fm^{-3}. Beyond the critical value, the pairing energy in the RMF+BCS model increases rapidly and approaches that in the RMF+FBCS model in the region of the strong pairing limit ($V_0 = 300 \sim 500$ MeV fm^{-3}). When the pairing strength exceeds 350 MeV fm^{-3}, the BCS pairing energy even becomes slightly larger than that in the FBCS model, due to the self-consistent nature of the calculations.

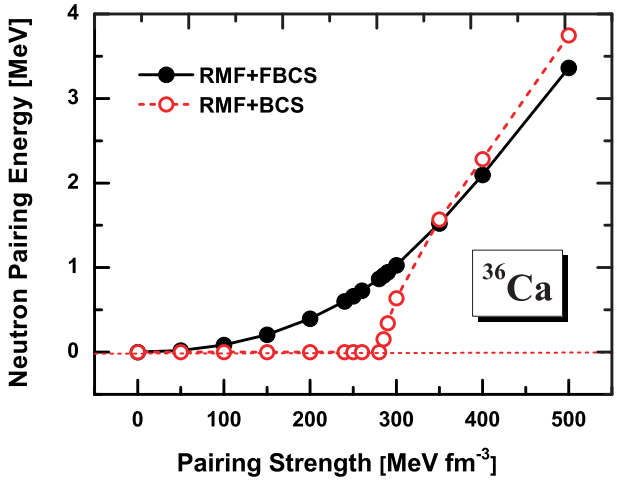

Fig. 1. (color online) Neutron pairing energy of ^{36}Ca as a function of the pairing strength.

Now we proceed to study the whole calcium isotopic chain from ^{32}Ca to ^{74}Ca. Two issues of particular interest are the magnitude of the pairing correlation and how it evolves as a function of the neutron (mass) number. One can define many different quantities for such a purpose [15]. Here we use the pairing energy defined in Eq. (17). In Fig. 2, we compare the neutron pairing energy of the calcium isotopes $^{32-74}$Ca obtained from the RMF+FBCS and RMF+BCS calculations with pairing strengths $V_0 = 300$ MeV fm^{-3} and $V_0 = 400$ MeV fm^{-3}, respectively. It is clear that the neutron pairing ener-

gies obtained with different pairing strengths show almost the same pattern. Particularly interesting is that at $N=14$, 20, 28, 32 and 40, the neutron pairing energy is smaller than that of their neighbors in the RMF+FBCS model. The same scenario occurs in the RMF+BCS model except for $N=32$ with $V_0=300$ MeV fm^{-3}, where the pairing energy vanishes. This shows that not only the conventional magic numbers $N=20$, 28, but also $N=14$, 40, and to a lesser extent $N=32$, show some kind of "magicity", which seems to agree with Refs [47–50].

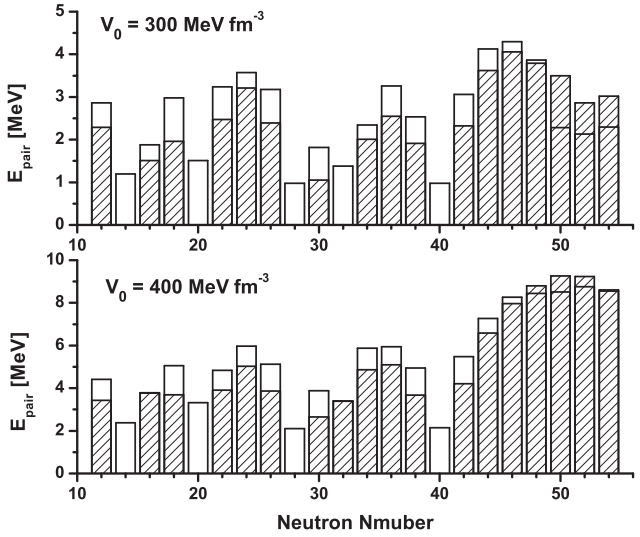

Fig. 2. Neutron pairing energies of the calcium isotopes as a function of neutron number with pairing strengths V_0=300 MeV fm^{-3} and V_0=400 MeV fm^{-3}, respectively. The results from the RMF+FBCS model (empty columns) are compared with those from the RMF+BCS model (shaded columns).

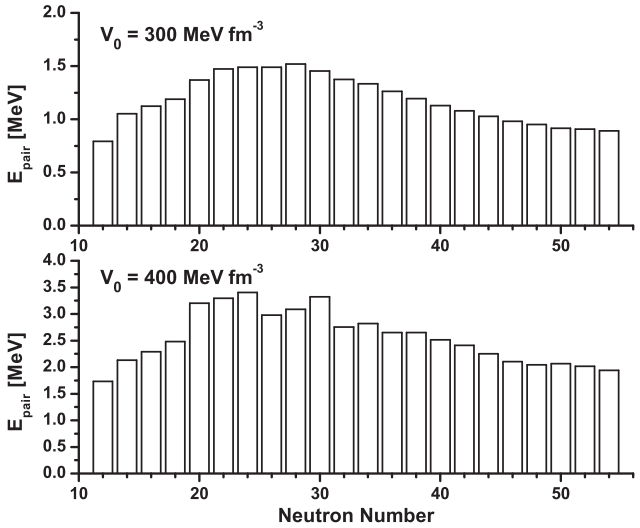

Fig. 3. Proton pairing energies of the calcium isotopes as a function of neutron number with pairing strengths V_0=300 MeV fm^{-3} and V_0=400 MeV fm^{-3}, respectively. The results from the RMF+FBCS model (empty columns) are compared with those from the RMF+BCS model (shaded columns).

In Fig. 3, we show the proton pairing energies of the calcium isotopes as a function of the neutron number. It can be seen that the RMF+FBCS pairing energies are still not zero, even for the proton magic number $Z=20$, which is different from those in the RMF+BCS calculations. Furthermore, the proton pairing energies vary slowly as a function of the neutron number, but the magnitude of this variation is small.

6 Ground-state properties of calcium isotopes

In this section, we study how the bulk ground-state properties of the calcium isotopes can be described in the RMF+FBCS and RMF+BCS models. The pairing strength is fixed at $V_0=350$ MeV fm^{-3} in the RMF+BCS model, and that in the RMF+FBCS model is fixed at $V_0=274$ MeV fm^{-3} by fitting to the odd-even mass differences of the whole calcium isotopic chain, defined as the following [15, 16]:

$$\Delta^{(3)}(N,Z)=B(N-1,Z)-2B(N,Z)+1/2B(N+1,Z). \tag{23}$$

In Fig. 4, the odd-even mass differences of the calcium isotopes calculated by the RMF+FBCS and RMF+BCS models are compared with the experimental data [51]. Both approaches reproduce the experimental data quite well, except for ^{40,48}Ca in the FBCS method. This can easily be understood because in the determination of the RMF parameters, doubly magic nuclei are supposed to have no pairing. More discussion can be found below.

Firstly, we examine the two-neutron separation energy, defined as the following:

$$S_{2N}(Z,N)=B(Z,N)-B(Z,N-2), \tag{24}$$

where $B(Z,N)$ is the binding energy of a nucleus with proton number Z and neutron number N. In the upper panel of Fig. 5, the two-neutron separation energies obtained from both models are compared with their experimental counterparts [51]. In the lower panel, the deviations of the theoretical two neutron separation energies from their experimental counterparts are shown. Except for $N=36$ and 38, the results of both methods agree quite well with the data . It seems that the $N=40$ magicity effect is overestimated in the RMF model.

A closer look at the two-neutron separation energies of ^{48}Ca, ^{50}Ca, ^{52}Ca and ^{54}Ca in Fig. 6 reveals that the experimental sharp drop from ^{52}Ca to ^{54}Ca is better reproduced in the RMF+FBCS model. The same scenario

is seen in the inset of Fig. 6, where there is a sharp drop from ^{70}Ca to ^{72}Ca in the RMF+FBCS model.

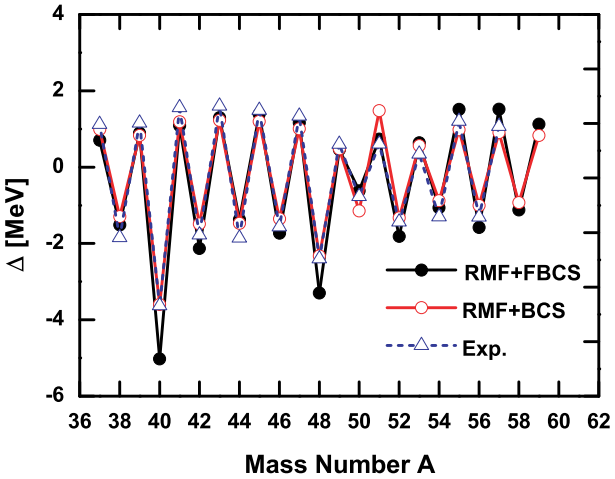

Fig. 4. (color online) Odd-even mass differences of Ca isotopes calculated by RMF+FBCS (full squares) and RMF+BCS (open squares) approaches in comparison with experimental data (open triangles) [51].

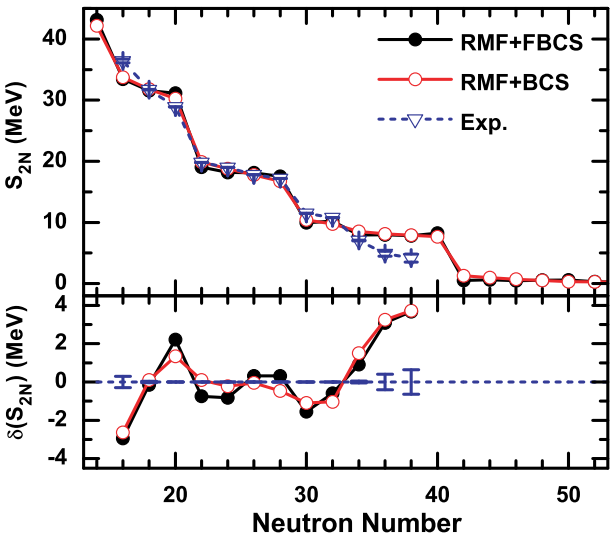

Fig. 5. (color online) Theoretical and experimental [51] two-neutron separation energies S_{2N} of the calcium isotopes and the difference between them, defined as $\delta(S_{2N})=S_{2N}(\text{th})-S_{2N}(\text{exp})$.

In Ref. [52], the pairing rotational moment of inertia is suggested to be an excellent pairing indicator, because odd-mass nuclei could contain the contribution from time-odd fields and be better avoided. The pairing rotational moment of inertia is proportional to the inverse of the two-nucleon shell gap indicator Δ_{2N} [53]:

$$\Delta_{2N}(Z,N)=2B(Z,N)-B(Z,N+2)-B(Z,N-2). \quad (25)$$

In Fig. 7, the two-neutron shell gaps of the calcium isotopes and the deviations from their experimental counterparts are plotted as a function of the neutron number. The RMF+BCS model provides a slightly better description of the experimental data, especially for ^{40}Ca and ^{48}Ca. This can easily be understood from the definition of Δ_{2N}. In the BCS method the pairing correlation is only effective on open-shell nuclei and reduces the two-neutron shell gaps of magic nuclei (compared with pure mean field models or the FBCS method).

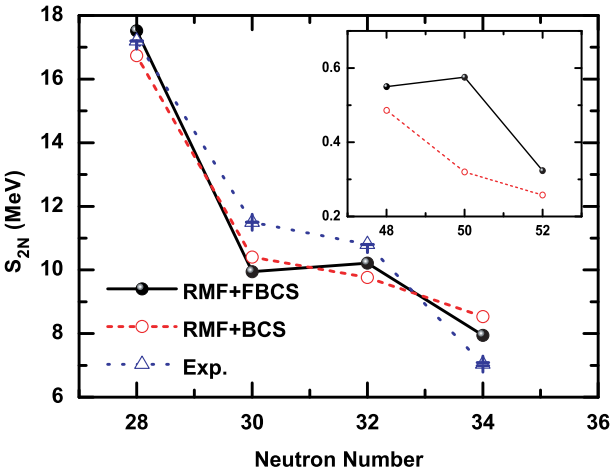

Fig. 6. (color online) Two-neutron separation energies of ^{48}Ca, ^{50}Ca, ^{52}Ca, and ^{54}Ca. The insert shows those of ^{68}Ca, ^{70}Ca, and ^{72}Ca.

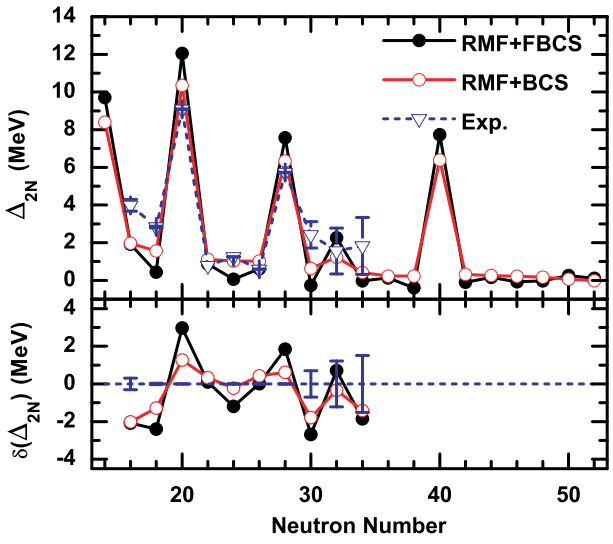

Fig. 7. (color online) Two-neutron gaps of the calcium isotopes and the differences between theoretical and experimental values [51] as a function of the neutron number.

From the studies of the two-neutron separation energies and two-neutron gaps of the calcium isotopes, it seems that the RMF+BCS calculations are of similar

quality or even slightly better than the RMF+FBCS calculations. This finding is not surprising. It is closely related to how we obtained the RMF parameters. The NL3 RMF parameterization is fitted to the ground-state properties of 10 magic or even-even nuclei [43]. That is to say, from the very beginning, we only expect the residual pairing correlation to make open-shell nuclei more bound but leave closed-shell nuclei unchanged. The BCS and Bogoliubov methods are perfect candidates to achieve this, as we can easily see in Fig. 3, though they break the gauge symmetry of particle number. In contrast, the FBCS method makes closed-shell nuclei more bound than the BCS or Bogoliubov method does and leaves open-shell nuclei more or less unchanged. Therefore, it is quite natural that no significant improvement has been observed. To really appreciate the FBCS method, in particular to improve the agreement with experimental data, the mean-field effective force has to be readjusted to leave room for incorporating these higher-order correlations [54]. Due to the present strategy used to fit the RMF parameters, at least part of the pairing effect for magic nuclei has been compensated by artificially large magic number effects at the order of several MeV.

In addition to the binding energies and related quantities, one can study the root mean square (r.m.s.) radii as well as the deformations of the calcium isotopes. We found that they are similar in both the RMF+BCS and RMF+FBCS models and therefore do not show them explicitly. On the other hand, we notice that close to the neutron drip line $N \geq 50$, the r.m.s. radii in the RMF+BCS model are slightly larger than those in the RMF+FBCS model, at the order of 0.05 fm. However, because of the harmonic oscillator basis adopted, we do not expect that either of our methods can properly describe the r.m.s. radii or the density distributions close to the neutron drip line. Nevertheless, we notice that the RMF+BCS and RMF+FBCS models can sometimes change the occupation probability of certain single particle levels close to the Fermi surface, and thus modify the density distributions. When the continuum states are more properly treated, this may have some impact on the spatial distributions of drip line nuclei. To illustrate this point, we investigate ^{54}Ca in detail below.

In the upper panel of Fig. 8, we plot the potential energy surface of ^{54}Ca as a function of the quadrupole deformation parameter β_{20}. The curves obtained in the two models look quite similar, both yielding a minimum at β_{20}=0, but the RMF+FBCS energy at large deformations becomes smaller. In the lower panel of Fig. 8, the neutron r.m.s. radius of ^{54}Ca is also shown as a function of β_{20}. Surprisingly, we see a bump in the center of the RMF+FBCS curve, different from the RMF+BCS case[1)].

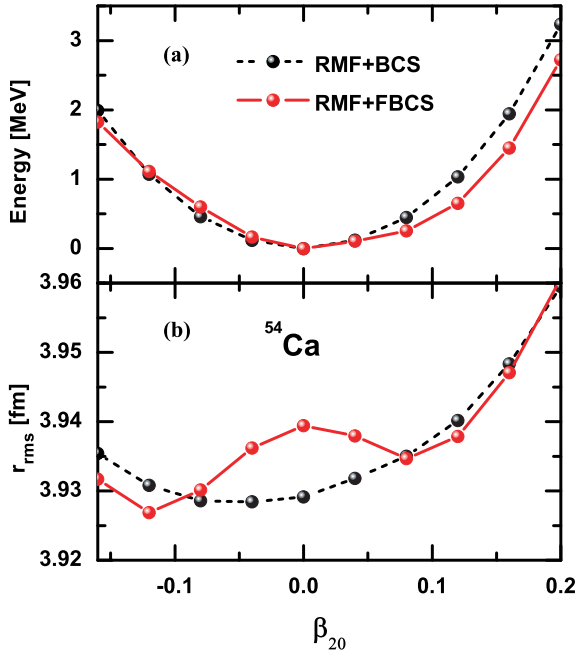

Fig. 8. (color online) Potential energy surface and root mean square radius of ^{54}Ca as a function of the deformation parameter β_{20} obtained in the RMF+BCS (dashed line) model and the RMF+FBCS (solid line) model.

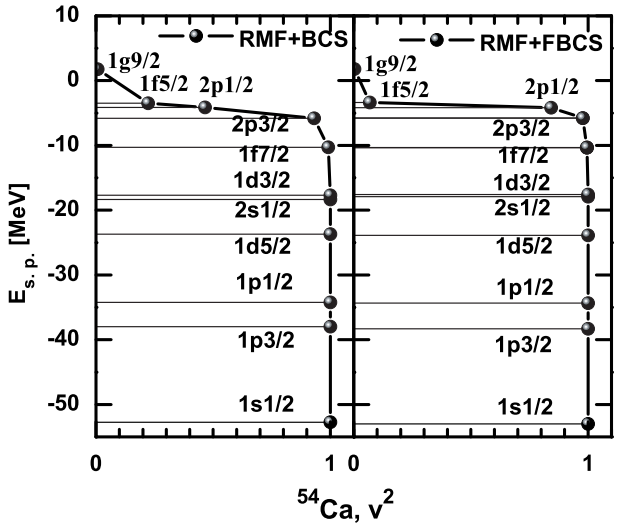

Fig. 9. (color online) Occupation probabilities of the neutron single particle levels of ^{54}Ca obtained in the RMF+BCS model (left) and the RMF+FBCS model (right).

1) We notice that increasing the pairing strength in the RMF+FBCS model will reduce the bump a little bit but the structure remains even for a pairing strength of 400 MeV fm^{-3}. In addition, the appearance of such a phenomenon also depends on the adopted mean-field parameters.

Since the binding energies at $\beta_{20}=0$ are similar to each other, such a difference can only originate from the different occupation probabilities of the single particle states close to the Fermi surface. This is indeed the case, as shown in Fig. 9. We see that the occupation probability of the neutron $2p_{1/2}$ state in the RMF+ FBCS is much larger than that of the RMF+BCS model. In the latter, more particles are scattered to the neutron $1f_{5/2}$ orbit. This explains why at $\beta_{20}=0$, the RMF+BCS and RMF+FBCS models predict a similar binding energy, but a different neutron r.m.s. radius.

In Fig. 10, we plot the contribution to neutron density from the neutron orbitals $1f_{5/2}$, $2p_{1/2}$ and $2p_{3/2}$. Clearly, in the two methods, the relative contributions from the $2p_{1/2}$ and $1f_{5/2}$ orbits are quite different. In the RMF+FBCS model, the contribution from the $2p_{1/2}$ orbit, which extends farther away from the center, is larger than that from the $1f_{5/2}$ orbit. In the RMF+BCS model, the opposite is true. These are the reasons behind the seemingly unusual behavior observed in Fig. 9.

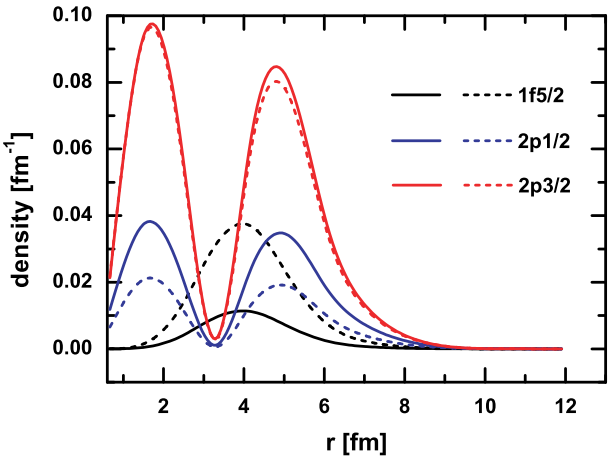

Fig. 10. (color online) Neutron density of the $1f_{5/2}$, $2p_{1/2}$, and $2p_{3/2}$ orbits of ^{54}Ca calculated in the RMF+FBCS (solid lines) and RMF+BCS (dashed lines) models.

7 Summary

We have formulated a particle number conserving BCS method, the so-called FBCS method, in the relativistic mean field model. We have shown that the RMF+FBCS model can properly describe the weak pairing limit. A detailed study of the calcium isotopes reveals that the RMF+FBCS results for the two-neutron separation energies and two-neutron gaps are similar to those of the RMF+BCS calculations; also, the density distributions are roughly the same in both calculations (and therefore not shown). Overall we do not find essential improvement in the description of the ground state properties of the calcium isotopes.

On the other hand, we notice that the neutron r.m.s radii at the neutron drip lines can be somewhat larger in the RMF+BCS model than in the RMF+FBCS model. In addition, our study has shown that the FBCS method can change the occupation probability of certain single particle orbitals around the Fermi surface and therefore affect the neutron r.m.s radius. For the case of ^{54}Ca, the increase of the radius is only about 0.02 fm, but this can be larger for more neutron-rich nuclei with similar configurations. However, due to the incorrect asymptotic behavior of the harmonic oscillator wave functions, the expansion in a localized HO basis is not appropriate for the description of drip line nuclei [55], particular for their density distributions. To treat the continuum more properly, one may solve the RMF model in coordinate space [7, 10] or adopt the Woods-Saxon basis [55, 56]. Implementing a particle number conserving BCS approach or Bogoliubov approach in such models and studying its impact on drip line nuclei would be of great interest both experimentally and theoretically. Such works are in progress.

An Rong and Shi-Sheng Zhang acknowledge valuable discussions with Prof. Shan-Gui Zhou of Institute of Theoretical Physics, Chinese Academy of Sciences.

References

1 Isao Tanihata, Herve Savajols, and Rituparna Kanungo, Prog. Part. Nucl. Phys., **68**: 215–313 (2013)
2 J. Meng and S. G. Zhou, J. Phys. G, **42**(9): 093101 (2015)
3 J. Dobaczewski, W. Nazarewicz, T. R. Werner, J. F. Berger, C. R. Chinn, and J. Decharge, Phys. Rev. C, **53**: 2809–2840 (1996)
4 J. Meng and P. Ring, Phys. Rev. Lett., **77**: 3963–3966 (1996)
5 W. Poschl, D. Vretenar, G. A. Lalazissis, and P. Ring, Phys. Rev. Lett., **79**: 3841–3844 (1997)
6 G. A. Lalazissis, D. Vretenar, W. Poeschl, and P. Ring, Phys. Lett. B, **418**: 7–12 (1998)
7 Jie Meng, Nucl. Phys. A, **635**(1 – 2): 3–42 (1998)
8 N. Sandulescu, Nguyen Van Giai, and R. J. Liotta, Phys. Rev. C, **61**: 061301 (2000)
9 Li-Gang Cao and Zhong-Yu Ma, Phys. Rev. C, **66**: 024311 (2002)
10 N. Sandulescu, L. S. Geng, H. Toki, and G. C. Hillhouse, Phys. Rev. C, **68**: 054323 (2003)
11 Li-Sheng Geng, Hiroshi Toki, Satoru Sugimoto, and Jie Meng, Prog. Theor. Phys., **110**: 921–936 (2003)
12 J. C. Pei, A. T. Kruppa, and W. Nazarewicz, Phys. Rev. C, **84**: 024311 (2011)
13 Shi-Sheng Zhang, En-Guang Zhao, and Shan-Gui Zhou, Eur. Phys. J. A, **49**(6): 77 (2013)
14 Ya-Juan Tian, Tai-Hua Heng, Zhong-Ming Niu, Quan Liu, and Jian-You Guo, Chin. Phys. C, **41**(4): 044104 (2017)
15 P. Ring and P. Schuck, The Nuclear Many-Body Problem, (New York: Springer-Verlag, 1980)
16 A.Bohr and B. R. Mottelson, Nuclear Structure, (Singapore: World Scientific, 1998)

17 John Bardeen, L. N. Cooper, and J. R. Schrieffer, Phys. Rev., **106**: 162 (1957)
18 John Bardeen, L. N. Cooper, and J. R. Schrieffer, Phys. Rev., **108**: 1175–1204 (1957)
19 Leon N Cooper et al, BCS: 50 years, (World Scientific, 2011)
20 N. N. Bogolyubov, Sov. Phys. JETP, **7**: 41–46 (1958); [Front. Phys., **6**: 399 (1961)]
21 Klaus Dietrich, Hans J. Mang, and Jean H. Pradal, Phys. Rev., **135**: B22–B34 (1964)
22 D. J. Dean and M. Hjorth-Jensen, Rev. Mod. Phys., **75**: 607–656 (2003)
23 Javid A. Sheikh and Peter Ring, Nucl. Phys. A, **665**(1 - 2): 71–91 (2000)
24 J. A. Sheikh, P. Ring, E. Lopes, and R. Rossignoli, Phys. Rev. C, **66**: 044318 (2002)
25 M. Anguiano, J. L. Egido, and L. M. Robledo, Nucl. Phys. A, **696**(3 - 4): 467–493 (2001)
26 M. Anguiano, J. L. Egido, and L. M. Robledo, Phys. Lett. B, **545**: 62–72 (2002)
27 Michael Bender, Paul-Henri Heenen, and Paul-Gerhard Reinhard, Rev. Mod. Phys., **75**: 121–180 (2003)
28 T. Nikšić, D. Vretenar, and P. Ring, Phys. Rev. C, **73**: 034308 (2006)
29 T. Nikšić, D. Vretenar, and P. Ring, Phys. Rev. C, **74**: 064309 (2006)
30 Wei-Chia Chen, J. Piekarewicz, and A. Volya, Phys. Rev. C, **89**(1): 014321 (2014)
31 Jie Meng, Jian-You Guo, Lang Liu, and Shuang-Quan Zhang, Front. Phys. China, **1**: 38 (2006)
32 Ming-Jian Cheng, Lang Liu, and Yi-Xin Zhang, Chin. Phys. C, **39**(10): 104102 (2015)
33 Z. Shi, Z. H. Zhang, Q. B. Chen, S. Q. Zhang, and J. Meng, Phys. Rev. C, **97**: 034317 (2018)
34 J. D. Walecka, Ann. Phys., **83**: 491–529 (1974)
35 P. G. Reinhard. Rept. Prog. Phys., **52**: 439 (1989)
36 Brian D. Serot and John Dirk Walecka, Adv. Nucl. Phys., **16**: 1–327 (1986)
37 P. Ring, Prog. Part. Nucl. Phys., **37**: 193–263 (1996)
38 J. Meng, H. Toki, S. G. Zhou, S. Q. Zhang, W. H. Long, and L. S. Geng, Prog. Part. Nucl. Phys., **57**: 470–563 (2006)
39 D. Vretenar, A. V. Afanasjev, G. A. Lalazissis, and P. Ring, Phys. Rept., **409**: 101–259 (2005)
40 J. Meng, Relativistic density functional for nuclear structure, volume 10, (World Scientific, 2016)
41 Y. K. Gambhir, P. Ring, and A. Thimet, Annals Phys., **198**: 132–179 (1990)
42 P. Ring, Y. K. Gambhir, and G. A. Lalazissis, Comput. Phys. Commun., **105**: 77–97 (1997)
43 G. A. Lalazissis, J. König, and P. Ring, Phys. Rev. C, **55**: 540–543 (1997)
44 Y. Sugahara and H. Toki, Nucl. Phys. A, **579**(3): 557–572 (1994)
45 Wen-Hui Long, Jie Meng, Nguyen Van Giai, and Shan-Gui Zhou, Phys. Rev. C, **69**: 034319 (2004)
46 Chin W. Ma and John O. Rasmussen, Phys. Rev. C, **16**: 1179–1195 (1977)
47 A. Gade et al, Phys. Rev. C, **74**: 021302 (2006)
48 F. Wienholtz et al, Nature, **498**(7454): 346–349 (2013)
49 Marcella Grasso, Phys. Rev. C, **89**: 034316 (2014)
50 Jia Jie Li, Jér?me Margueron, Wen Hui Long, and Nguyen Van Giai, Phys. Lett. B, **753**: 97–102 (2016)
51 W. J. Huang, G. Audi, Meng Wang, F. G. Kondev, S. Naimi, and Xing Xu, Chin. phys. C, **41**(3): 30002 (2017)
52 Nobuo Hinohara and Witold Nazarewicz, theory. Phys. Rev. Lett., **116**: 152502 (2016)
53 D. Lunney, J. M. Pearson, and C. Thibault, Rev. Mod. Phys., **75**: 1021–1082 (2003)
54 P. H. Heenen, A. Valor, M. Bender, P. Bonche, and H. Flocard, Eur. Phys. J. A, **11**: 393–402 (2001)
55 Shan-Gui Zhou, Jie Meng, and P. Ring, Phys. Rev. C, **68**: 034323 (2003)
56 Shan-Gui Zhou, Jie Meng, P. Ring, and En-Guang Zhao, Phys. Rev. C, **82**: 011301 (2010)